Practical Analysis of Radar Interference in a Communications System

BY

MANAS NYATI
B.Tech., Rajasthan Technical University, 2015

THESIS

Submitted as partial fulfillment of the requirements
for the degree of Master of Science in Electrical and Computer Engineering
in the Graduate College of the
University of Illinois at Chicago, 2018

Chicago, Illinois

Defense Committee:

        Danilo Erricolo, Chair and Advisor
        Daniela Tuninetti
        Natasha Devroye
        Besma Smida
        Ahmad Salim (Post-Doctoral Research Assistant)

to the faith...

ACKNOWLEDGMENTS

TABLE OF CONTENTS

TABLE OF CONTENTS (Continued)

LIST OF TABLES

LIST OF FIGURES

LIST OF ABBREVIATIONS

SNR   Signal to Noise Ratio

INR   Interference to Noise

BW   Bandwidth

BER   Bit Error Rate

EVM   Error Vector Magnitude

PW   Pulse Width

PRI   Pulse Repetition Interval.

SUMMARY

Spectrum sharing is a must in a world of revolution with wireless technology. It is critical to develop methodologies which aim at reducing the interference caused by these wireless technologies, operating especially in the same frequency bands. Radar operating in S-Band degrades the performance of commercial communications system, hence this research presents a novel method to analyze the data of a real-time model developed using Keysight Signal Analyzer and Signal Generator. In principle, spectrum sharing could occurs at all frequencies, but we have investigated the S-band where a plethora of applications exist on the commercial front. For the very same, various test cases were observed and theoretical formula were proposed to justify the results. This research also aims at comparing the experimental results to the analytical and simulation ones using Jensen-Shannon Divergence (JSD) and it proves that our proposed model is a good approximation to the joint the radar-communications system.

CHAPTER 1

INTRODUCTION

Increase in the heavy usage of wireless networks and radar systems have urged the need for efficient spectrum sharing. Technical parameters for both the systems are limited by the spectrum allocations, hence this research addresses this issue by presenting the novel experimental model to understand S-Band (from 2 GHz to 4 GHz) radar interference in an uncoded communications system. This real-time model was developed using Keysight signal analyzer and signal generator. Consequently, a number of parameters were varied and test cases were evaluated, especially bit-error-rate performance to underline the appropriate requirement for the radar to coexist with the communications system. The adopted method was also compared with ideal cases and verified with a brief theoretical analysis.

The radar interference could affect the performance of a communications system hence it is challenging to develop a co-existence system. Many authors have proposed methods that address this issue and have presented their ideas either using a simulated environment or through experiments. For simulated/theoretical concepts, in order to minimize the interference, (1) develops a channel selection algorithm and NSP (null-space projection) algorithm which choose the best way in which the the radar could project its signals. (2) aimed at modifying the transmitter and receiver of 802.11 wireless local area network WLAN communications system with the column inter-leaver and LLR (long likelihood ratio) mapping function so as to successfully deal with the radar interference. This model was built in MATLAB 2015 WLAN toolbox based on the IEEE 802.11ac standard because there was a need to model the simulated environment into the practical world.

1

Experimentally, for the communications system, many people proposed the use of real-time devices like USRP (Universal Software for Radio Peripheral) to implement BPSK, 4-QAM, OFDM and other types of modulation algorithms. These radio transceivers were meant to develop a real-time model within the lab setup like (3)(4) with LabVIEW serial interface (3). Since these devices are un-calibrated and prone to high noise figure, these devices are not perfect tools to perform any kind of analysis such as bit error tests, error vector magnitude test etc. Thus, more sophisticated devices like the ones used in (5) were implemented. These signal analyzer and the signal generator have an ability to perform the analysis like bit error rate (BER) calculations with much greater accuracy and with very low tolerance values. These devices were used to test the S-Band radar spectrum sharing methods and their co-existence with the LTE network or the mobile network and proved experimentally that the degradation of the performance is caused at each end, for both communications system and the radar system.

This research interests in proving the results of theoretical and simulated study experimentally. This research targets to be an extension to (6)(7)(8) which have analytically studied the effect of the radar interference in a single carrier communications system. (7) develops a relation between the signal to noise ratio (SNR), interference to noise ratio (INR), BER and considers three regimes (INR$\ll$SNR, INR$\approx$SNR, and INR$\gg$SNR) to analyze the interference results theoretically. Similarly, (9) proves theoretically that low power communication interference can degrade the radar performance significantly and communication interference should not be modeled as the Gaussian interference of the same power which is a good approximation in general. Though some author have proposed the Gaussian mixture distribution (10) to model the impulsive radar signal in the form of DME shaped pulse and then optimize the receiver based on analysis, but lacks the experimental proof. Therefore, an attempt was made

to prove those theoretical results experimentally using real-time devices or devices which could mimic

radio transceivers.

TABLE I: Notations and symbols

P_r	Radar system transmit power (dBm)
P_c	Commumications system transmit power (dBm)
F_r	Radar system center frequency (Hz)
F_c	Commumications system center frequency (Hz)
τ_R	Radar pulse width (s)
T_{PRI}	Radar pulse repetition interval (s)
B_c	Bandwidth of communications system (Hz)
B_r	Bandwidth of radar system (Hz)
SNR	Signal to noise ratio (dB)
INR	Interference to noise ratio (dB)
BER	Bit error rate ratio
EVM%	Error vector magnitude percentage

Using the knowledge about the past work (7)(11), this research will in detail explain its contributions and its implications in real-world to minimize the radar interference in the communications system. Though past work like (6)(8)(11) did characterize the joint model of radar-communicaitons system analytically and also proposed a way to calculate BER with varying radar and communications system power, but we are not aware of any other work which attempt to experimentally prove the analytical characterization. There are two important aspects which make this research different from the work done previously: 1)Novel lab-setup and 2)In-depth analysis considering different test cases. Since pulse width τ_R, pulse repetition interval PRI, frequency F_r and power P_r define the nature of the radar pulse or in other words the interference (refer I for notations) , their variation is an important aspect in order to study its impact on a communications system. Also, one needs to keep in mind parameters such as P_c, F_c and bandwidth BW of the communications system, since they also play an important role to determine how "powerful" the impact of interference could be. The major findings for the test setup for the radar and communications system include:

- For the communications system alone, BER performance for different SNR using BPSK and 4-QAM modulation followed the ideal "waterfall" graph.

- For the radar system alone with a simple rectangular pulse train, we observed interesting "circles" or "circular rings" at the center of IQ diagram which could be also explained by a deterministic linearly changing phase with time. The circle's radius R varies with the change in the radar F_r, it's P_r and τ_R. The circle's radius R and its ring "scattering" somehow depicts how strong or weak the interference signal is. For example, the value of R increased when P_r was changed from -20 dBm to -10 dBm, while keeping other parameters constant.

We varied numerous values, for example, the radar pulse width (PW), pulse repetition interval (PRI), the radar power (P_r) or Interference to noise ratio (INR), etc. and have successfully analyzed the results with their real-life applications. For the joint radar-communications system, mostly spectrum, IQ vector and BER analysis were done with test cases considering variation in parameters such as P_c, P_r, T_{PRI}, F_r, B_c and B_r and their few possible combination. Following were the major findings:

- The EVM% and BER values increased significantly with a variation of F_r, keeping the other values constant. For example, the BER value increased by a factor of 10 with a -10 dBm power change of the radar signal.

- The BER increased when F_r was brought closer to F_c, keeping the other parameters unchanged. For example, BER of 4.4×10^{-3} was computed with $\Delta F = F_c - F_r$ as 680 Hz and for $\Delta F = 20$ Hz, BER increased to 0.45. The radius R of circles also increased when F_r was moved closer to F_c.

- With the same setup, it was observed that the PRI and BER followed an inverse linear relation. For example, increasing PRI from 100 μs to 500 μs decreased the BER from 3.1×10^{-2} to 6.3×10^{-3}.

- Simultaneous variation in B_c and B_r by the same amount had no effect on the BER. For example, there was a constant BER when reference B_c=500 MHz and B_r=1 MHz were made half or twice of their respective values.

In the later chapters, we will perform analysis of interfering radar signal at the receiver of a communications system which uses binary phase shift keying (BPSK) demodulation.Similar to (12), which performed analysis for OFDM system, we will consider different radar pulses and their probability mass functions (PMFs).The joint PMFs for the amplitude and phase were also derived. These analytical PMFs

are then compared to the simulation and experimental (only for the case of rectangular radar pulse) results using Jensen Shannon divergence (JSD) (13)(14) to measure the distance between them. We will see that our experimental setup matches closely with the proposed simulation and the analytical setup.

1.1   Experimental Setup

The experimental setup consisted of the following arrangement in an Anechoic room as shown in 1 with communications system separated by 2.69 m distance and the radar antenna placed at an angle of 38 degrees and 1.69 m distance from communications receiver. The orientation of the antenna is aligned to match the polarization of the transmitted communications signal. For most cases, test frequency for the communications system was F_c=2.849520 GHz and for the radar system was F_r=2.85 GHz, as used in (12).

Sophisticated devices with compatible software were used in our experimental set-up:

- Keysight N5172B EXG VSG Vector Signal Generator (as communications transmitter).

- Keysight N5172B EXG VSG Vector Signal Generator (as the radar transmitter).

- Keysight N9020B MXA SA Signal Analyzer (as communications receiver).

- Keysight 89600 VSA 22.2 (to evaluated BER, EVM%, etc of the received signal)

- Keysight Signal Studio IQ Toolkit (to configure the communications and the radar transmitted signal)

- Keysight Command Expert CE (to play/acquire the signals from the devices)

- MATLAB (for computational purposes)
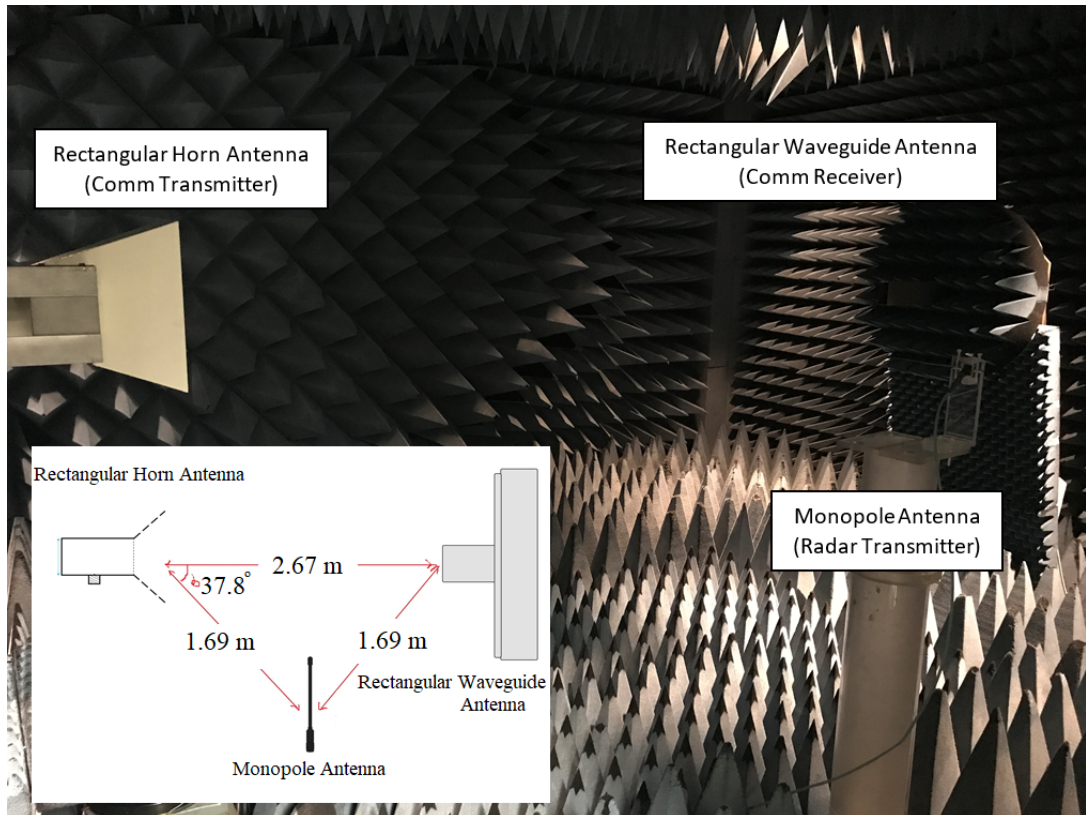
Figure 1: Experimental setup in an anechoic chamber with the antennas were positioned as shown. The distance between the communications system is 2.67 m and the distance between the communications receiver and the radar monopole antenna is 1.69 m.

To model the joint radar-communications system, this research used VSG as transmitter and SA as a receiver with another VSG as an interference unit. User-known random bits were generated with the help of VSG, which transmitted the bits at different frequencies, amplitude levels, and the modulation types. The received signal at SA was analyzed by evaluating the RF envelope waveform in the time domain, spectrum, constellation diagram, etc. using VSA and MATLAB. GPIB or Ethernet cable made
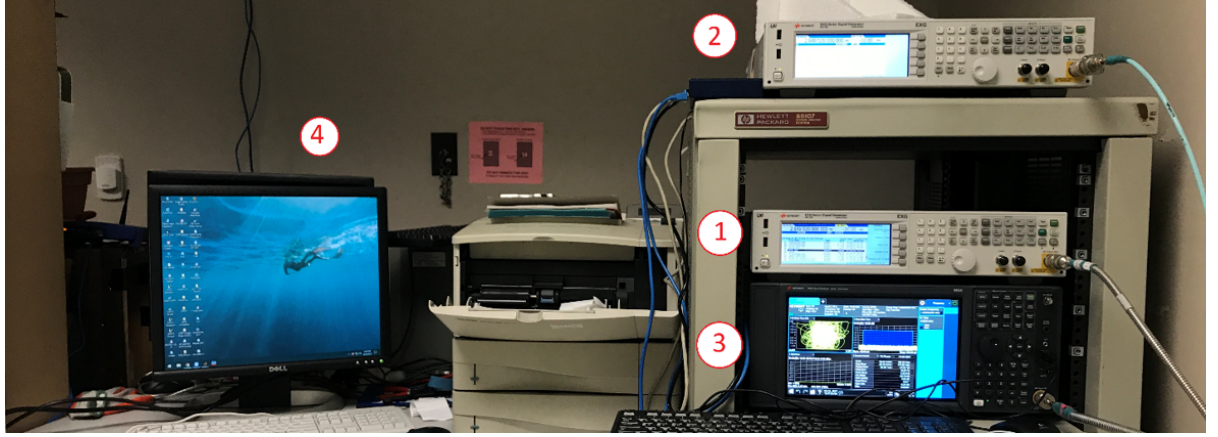
Figure 2: Bench-setup for experiments: 1. Vector Signal Generator (as communications transmitter), 2. Vector signal generator (as the radar transmitter), 3. Signal Analyzer (as communications receiver),4. Interfacing software and windows. Note that the cables from the devices were passed through the anechoic chamber and all the transmission and reception took place inside the chamber.

it easier to communicate with these devices via PC. We evaluated the data for numerous cases, such as communications alone setup, the radar alone set up, and communications-radar co-existence setup, by observing the received and the transmitted signal.

1.2 Theory

Consider a general radar pulsed signal operating at central frequency F_r Hz with a pulse width of τ_R s. PRI of the passband radar signal $Y(t)$ is given by T_{PRI} s. Also taken into account is the delay/lag time t_d s between the communications system and the radar signal. Sampling frequency at the communications system is $F_s = \frac{1}{T_s}$ where T_s is the sampling period. A similar analysis was also carried out in (12).

1.2.1 Transmitted Signal

Consider a radar pulse A(t) with a time t and amplitude varying signal A_m(t) for the pulse width dura-tion. Here m denotes the different pulse shape, i.e, for example, rectangular, chirp, Distance Measuring Equipment (DME) pair pulse, etc. The total number of pulses taken was N.

$$A(t) = \begin{cases} A_m(t), & \text{for } c_i \leq t \leq d_i \\ 0, & \text{elsewhere} \end{cases}, \forall n_i \in [0, N-1]$$

where, $c_i = n_i T_{PRI}$, $d_i = n_i T_{PRI} + \tau_R$ and n_i is the index of the nth radar pulse.

The signal A(t) is upcoverted by multiplying it by the carrier signal, $e^{j2\pi F_r t}$. Since the radar signal lags the communications system by the delay t_d, the passband radar signal can be written as

$$Y(t) = \Re\{A(t-t_d)e^{j2\pi F_r(t-t_d)}\} \tag{1.1}$$

$$= A(t-t_d)cos(2\pi F_r(t-t_d)) \tag{1.2}$$

Similarly, if m(t) is the BPSK or QPSK modulated signal, then the passband $s_P(t)$ could be defined as

$$s_P(t) = \Re\{m(t)e^{j2\pi F_c t}\} \tag{1.3}$$

1.2.2   Received Signal

At the communication receiver, the received passband signal of the radar (1.2), as well as commu-

nications signal (1.3) are downcoverted using the communications system carrier frequency F_c and it

is sampled at frequency F_s. The downconverted signal $Y_d[n]$ passes through an IF or a low pass filter

resulting in the baseband signal R[n], where n is the index of the nth sample. Assuming the bandwidth

of the radar is less than that of communications system, the downconverted sampled signal could be

expressed as

$$Y_d[n] = Y(nT_S)e^{-j2\pi F_c nT_S} + \mathcal{N} \tag{1.4}$$

$$= \frac{1}{2}A(nT_S - n_d T_S)[e^{j(2\pi(F_r - F_c)nT_S - 2\pi F_r n_d T_S)}$$

$$+ e^{-j(2\pi(F_r + F_c)nT_S - 2\pi F_r n_d T_S))}] + M(nT_S) + \mathcal{N} \tag{1.5}$$

Here $n_d = \lfloor \frac{t_d}{T_S} \rfloor$, which is assumed to be uniformly distributed as $n_d \sim \mathcal{U}\left\{\left[0 : \frac{T_{\mathrm{PRI}} - \tau_R}{T_S}\right]\right\}$ (12) with

T_{PRI}, τ_R and T_C (which is symbol spans in seconds) as multiples of T_S. Also, it was assumed that $T_{PRI} = T_C$

and $\mathcal{N}$ to be AWGN noise. Following this, the high frequency component namely, $(F_r + F_c)$ is filtered

by the low pass filter of IF stage centered around F_c, assuming it to be an ideal with unity gain for the

simplicity. Hence the baseband signal R[n] is expressed as

$$R[n] = \frac{1}{2}A(nT_S - n_d T_S)[e^{j(2\pi(F_r - F_c)nT_S - 2\pi F_r n_d T_S)}]$$

$$+ M'(nT_S) + \mathcal{N}_F \tag{1.6}$$

or simply,

$$R = Ie^{j\Theta} + S + \mathcal{N}_F \tag{1.7}$$

where,

$$I = \frac{1}{2}A(nT_S - n_d T_S), \tag{1.8}$$

$$\Theta = 2\pi(F_r - F_c)nT_S - 2\pi F_r n_d T_S, \tag{1.9}$$

$$S = M'(nT_S) \tag{1.10}$$

In 1.7, $Ie^{j\Theta}$ could be treated as baseband radar signal before demodulation at the communication receiver with an amplitude I and random phase Θ where $\Theta \sim \mathcal{U}\{[b, a+b]\}$. Here a=-$2\pi F_r T_S$ and b= $2\pi(F_r - F_c)nT_S$. S could be defined as the received communication signal with an amplitude υ. $\mathcal{N}_F$ is the correlated coloured noise at the output of filter or in another words, noise present in the system after the IF stage defined by autocorrelation function as $\phi_{nn}(f) = N_o W \operatorname{sinc}(2W_\tau)$ if the input noise spectral density is $\phi_{ww}(f) = \frac{N_o}{2}$ considering an ideal filter. We analyzed this system using real-time test models and performed computations for various cases discussed in the later chapters.

For the next chapter, we will be discussing about an analytical model which describes a radar pulse at the communications receiver. We used the equation $R = Ie^{j\Theta} + S + \mathcal{N}_F$, which describes joint radar-communications setup, to compare and propose the results we got from the experiments.

CHAPTER 2

ANALYTICAL MODEL OF THE RADAR SIGNAL AT THE COMMUNICATIONS RECEIVER

Previous sections gave an insight about the idea behind modeling a real-time system. This section analyzes the effect of interfering radar signal at the receiver of a communications system, which used binary phase shift keying (BPSK) demodulation. Different radar pulse were considered and their probability mass functions (PMFs) as well as joint PMFs for the amplitude and phase of the baseband received radar pulse were derived. These analytical PMFs were compared to the simulated and experimental results using Jensen Shannon divergence which measured the directed divergence between the distributions.

For the analysis, we considered that general radar pulsed signal operates at F_r Hz with a pulse width of τ_R s. The pulse repetition interval of the passband radar signal $Y(t)$ is given by T_{PRI} s. Also taken into account is the delay/lag time t_d s between the communications system and the radar signal. Sampling frequency at the communications system is $F_s = \frac{1}{T_s}$ where T_s is the sampling period. Here, we assumed that the time delay t_d s was uniformly distributed random variable over $[0, (T_{PRI} - \tau_R)]$.

2.1   Radar transmission system (Radar pulse generation)

Consider a radar pulse $A(t)$ with a time and amplitude varying signal $A_m(t)$ for the pulse width duration. Here m denotes the different pulse shape, i.e, for example rectangular, chirp, Distance Measuring Equipment (DME) pair pulse, etc. The total number of pulses taken are N.

$$A(t) = \begin{cases} A_m(t), & \text{for } c_i \leq t \leq d_i \\ 0, & \text{elsewhere} \end{cases}, \forall n_i \in [0, N-1]$$

where, $c_i = n_i T_{PRI}$, $d_i = n_i T_{PRI} + \tau_R$ and n_i is the index of the nth radar pulse.

The signal $A(t)$ was upcoverted by multiplying it by the carrier signal, $e^{j2\pi F_r t}$. Since the radar signal lags the communications system by the delay t_d, the passband radar signal can be written as

$$Y(t) = \Re\{A(t - t_d)e^{j2\pi F_r(t - t_d)}\} \tag{2.1}$$

$$= A(t - t_d)cos(2\pi F_r(t - t_d)) \tag{2.2}$$

2.2   Communication receiver system (Radar pulse reception)

At the communication receiver system, the received passband signal is downcoverted using the communications system carrier frequency F_c and it is sampled at frequency F_s. The downconverted signal $Y_d[n]$ was passed through a low pass filter resulting in the baseband signal $R[n]$ before demodulation,

where n is the index of the nth sample. Considering the bandwidth of the radar to be larger than that of communcations system, the downconverted sampled signal was given by

$$Y_{\mathrm{d}}[n] = Y(nT_S)e^{-j2\pi F_c nT_S} + \mathcal{N} \tag{2.3}$$

$$= \frac{1}{2}A(nT_S - n_d T_S)[e^{j2\pi(F_r-F_c)nT_S - F_r n_d T_S}$$

$$+ e^{-j2\pi(F_r+F_c)nT_S - F_r n_d T_S}] + \mathcal{N} \tag{2.4}$$

Here $n_d = \lfloor \frac{t_d}{T_S} \rfloor$, which was assumed to be uniformly distributed as (12) where the value of $n_d \sim \mathcal{U}\left\{\left[0 : \frac{T_{\mathrm{PRI}}-\tau_R}{T_S}\right]\right\}$ with T_{PRI}, τ_R and T_C (which is symbol spans in seconds) were multiples of T_S. Also, it was assumed that $T_{PRI}=T_C$. Following this, the high frequency component namely $(F_r + F_c)$, was filtered by the low pass filter centered around F_c, assuming it to be ideal with unity gain for simplicity. Hence the baseband signal R[n] was expressed as

$$R[n] = \frac{1}{2}A(nT_S - n_d T_S)[e^{j2\pi(F_r-F_c)nT_S - F_r n_d T_S}] + \mathcal{N}_F \tag{2.5}$$

$$\boxed{R[n] = \frac{1}{2}\alpha e^{j\beta} + \mathcal{N}_F} \tag{2.6}$$

or,

$$\boxed{R[n] = M[n] + \mathcal{N}_F} \tag{2.7}$$

where,

$$\alpha = A(nT_S - n_d T_S), \tag{2.8}$$

$$\beta = 2\pi(F_r - F_c)nT_S - F_r n_d T_S, \tag{2.9}$$

$$M[n] = \frac{1}{2}\alpha e^{j\beta} \tag{2.10}$$

In 2.6, $\mathcal{N}_F$ was the correlated coloured noise at the output of filter or in another words, noise present in the system after the IF stage defined by autocorrelation function as $\phi_{nn}(f) = N_o W \operatorname{sinc}(2W_\tau)$ if the input noise spectral density was $\phi_{ww}(f) = \frac{N_o}{2}$ considering an ideal filter. The symbols α and β represents the amplitude and the phase of the received baseband signal before demodulation, respectively. Also, M[n] was the signal of interest without noise, or in other words it could be defined as the radar signal at the receiver without presence of noise. Since bandwidth of the system is considerably large, for our setup the filtered noise is assumed to be uncorrelated, following the IID property for the samples.

2.3   Rectangular radar pulse model and its analysis

Consider a rectangular radar pulse $A(t)$ with an amplitude ρ and total number of N pulses. Thus,

$$A(t) = \begin{cases} \rho, & \text{for } c_j \leq t \leq d_j \\ 0, & \text{elsewhere} \end{cases}, \forall n_i \in [0, N-1]$$

where, $c_j = (n_i T_{PRI})$, $d_j = (n_i T_{PRI} + \tau_R)$ and n_i is the index of the nth rectangular radar pulse. From the 2.7, the marginal and joint PMFs will be derived in the following subsections. From 2.7, first

distribution of signal M[n] will be calculated along with the distribution of filtered noise $\mathscr{N}_F$. Using random variables theorem, we will calculate the sum of these two distributions.

2.3.1 The PMF of the radar's amplitude

From 2.7, we can conclude that the amplitude of M[n] is α where,

$$\alpha = \begin{cases} \frac{\rho}{2}, & \text{for } \frac{n_i T_{PRI}}{T_S} + n_d \leq n \leq \frac{n_i T_{PRI} + \tau_R}{T_S} + n_d \\ 0, & \text{elsewhere} \end{cases} , \forall n_i \in [0, N-1]$$

Therefore,

$$\Pr(\alpha = \frac{\rho}{2}) = \frac{\tau_R}{T_{PRI}} \tag{2.11}$$

$$\text{and } \Pr(\alpha = 0) = \frac{T_{PRI} - \tau_R}{T_{PRI}} \tag{2.12}$$

As previously discussed, noise is assumed to be uncorrelated following the IID property for the samples, hence for the distribution of amplitude of $\mathscr{N}_F$ filtered response of AWGN noise will be accounted into. Since, for any filter with impulse response h(t), the filter output is also zero-mean Gaussian process. Also, we know the variance $\sigma_F{}^2$ of the filtered noise with response H(f) is given by,

$$\sigma_F{}^2 = \frac{N_0}{2} \int_{-\infty}^{\infty} |H(f)|^2 df \tag{2.13}$$

In other words, distribution of filtered noise $\mathscr{N}_F$ is a Gaussian distribution with

$$\mathcal{N}_F \sim \mathcal{N}\left(0, \frac{N_0}{2}\int_{-\infty}^{\infty}|H(f)|^2 df\right) \tag{2.14}$$

From 2.11 and 2.14, the total PMF R_X of the amplitude of R[n] could be described by

$$R_X = M_X * \mathcal{N}_F, \tag{2.15}$$

where M_X is the PMF of α. This expression was easily calculated via MATLAB while evaluating JSD.

2.3.2   The PMF of the radar's phase

Similar to the previous section, the distributions of R[n] and $\mathcal{N}_F$ were evaluated separately. From 2.7,$\angle R$ can be written as a $\tan^{-1}$ function of n_d as follows

$$\angle R = \tan^{-1}\frac{n_I + r_I}{n_Q + r_Q} \tag{2.16}$$

where, $e^{j\beta} = r_I + jr_Q$ and $\mathcal{N}_F = n_I + jn_Q$. Since $\mathcal{N}_F = n_I + jn_Q$ is a Gaussian distribution, the phase distribution of $\mathcal{N}_F$ will also be uniform. Considering large bandwidth, for the time duration of rectangular radar pulse it was computed that the PMF of phase was

$$\Phi \sim \mathscr{U}\,(b, a+b)$$

where, $a = -F_r T_S$ and $b = 2\pi(F_r - F_c)nT_S$.

2.3.3   The joint PMF of radar amplitude and phase

The joint PMF was written in the terms of the conditional PMFs. Simply put, the phase of the interference given a specific amplitude was uniformly distributed. The joint PMF was given by

$$P_{A,\theta}(a,\phi) = \mathbf{P}[A = a, \theta = \phi] = \mathbf{P}[\theta = \phi | A = a] \times P_A[a] \tag{2.17}$$

Similarly, the analysis for the marginal and joint PMFs of the different radar pulse shape like chirp, DME pulse pair, Gaussian, etc. were derived following the same steps as before. But for this section we limited ourselves to the detailed analysis for only one pulse. In the later sections, JSD of analytical, simulation and experimental setup have been compared for the different pulse shape and other reference values. Thus, in the next chapter we will look forward to the experimental setup and the various test cases for the measurements which will be utilized in the later chapters for measuring JSD values.

CHAPTER 3

TEST AND MEASUREMENT SOLUTIONS

Our approach to understanding the co-existence between the radar and communications systems was to first develop a reliable communications system using BPSK and 4-QAM modulation techniques, then transmit user-defined un-coded bits and compare the BER versus SNR of the setup with the ideal values. The results showed great resemblance to the ideal curve. Next, rectangular pulsed radar was introduced as interference to the existing communications system. Diverse cases considering variations in the values of the radar pulse width, pulse repetition interval, the radar power or interference to noise ratio, etc. were considered and analyzed.

3.1   Test for Communications System Alone

Bit error rate for different signal powers were computed for distinct values of P_c or signal-to-noise ratio at 1 MHz channel bandwidth (with 0.5 RRC shaping coefficient), F_c=2.84952 GHz followed with the BPSK and QPSK modulation scheme as per experimental setup shown in 1. The oscillator of VSG and SA were locked by a 10 MHz reference. Since the radar signal is turned off, this test case could be simplified further from 1.7 into $R = S + \mathcal{N}_F$.

3 shows the experimental and theoretical curves for BPSK and QPSK modulated communications system while evaluating BER versus SNR. Experimental data for two different modulations if closely matched followed the ideality which claims that for a given SNR, BER of the BPSK system is lower than that of the QPSK system. For example, the QPSK system gives the BER of 1.0×10^{-1}, which is
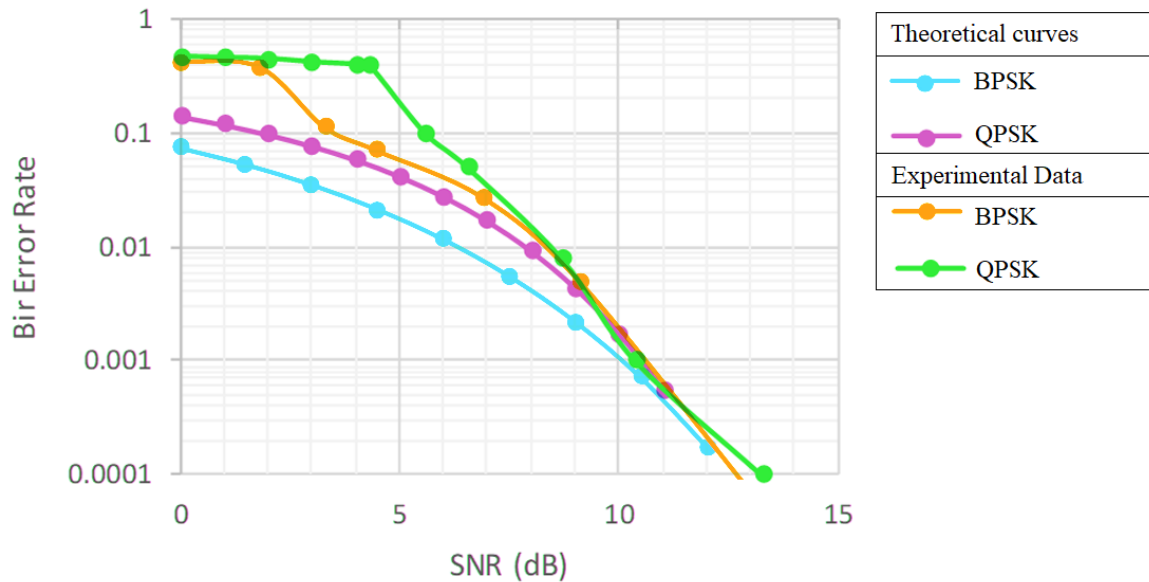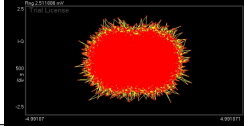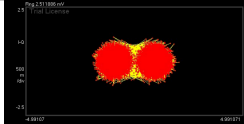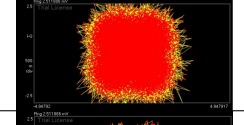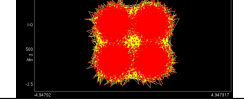
Figure 3: BER versus SNR "Waterfall" Graph for BPSK and QPSK Modulated Communications System

higher as compared with the 2.9×10^{-2} for BPSK system for the given transmitted power P_c=65 dBm. Therefore, for our setup, we could conclude that the reception for a BPSK communications system was better when the power transmitted P_c was greater than -63 dBm and it degraded significantly when the transmitted power was decreased.

In 3, we observed a significant deviation of curve w.r.t ideal curves below SNR levels of 2 to 3 dB for BPSK modulation and 4 to 5 dB for QPSK modulation. This could be explained by the receiver sensitivity, which made it difficult to extract/receive the signal of interest.

TABLE II: BER versus SNR evaluation for communications system

P_c(dBm)	SNR(dB)	BER	IQ Diagram
BPSK modulation technique			
-68	2.98	7.5×10^{-2}	
-60	8.596	8.7×10^{-5}	
QPSK modulation technique			
-65	5.578	1.0×10^{-1}	
-60	8.7	7.9×10^{-3}	

3.2 Test for Radar System Alone

The radar rectangular pulse signal alone, when passed through a communications system, gives interesting results. We have discussed the test case with varying radar amplitude in detail below.
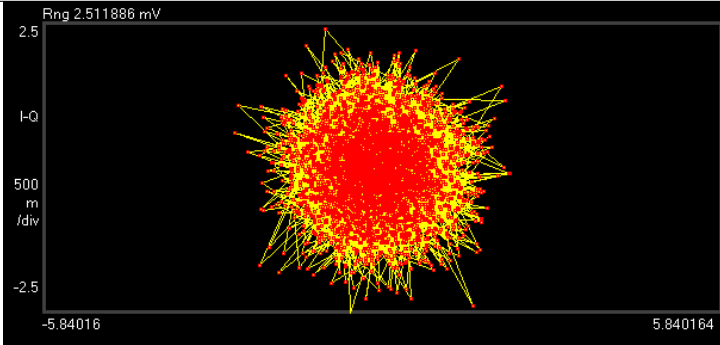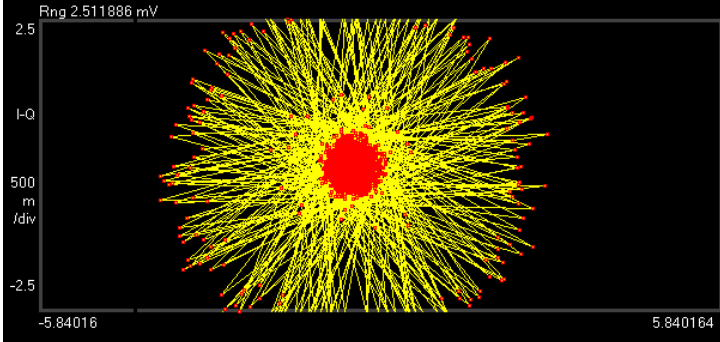
3.2.0.1 IQ Analysis for INR/P_r variation (τ_R, T_{PRI}=constant)

The radar signal alone from 1.7 could be defined as an interference signal with random noise incorporated in the background.

$$R = Ie^{j\theta} + N \tag{3.1}$$

Experiments to study the nature of the radar pulse at the communications receiver when transmitted at F_r=2.85 GHz but with variable transmitted radar power P_r were performed. The τ_R=10 μs and T_{PRI}=200 μs were kept the same for each iteration.

TABLE III: IQ Analysis for P_r Variation

P_r(dBm)	IQ Diagram
-50	
-30	

Some unique observations based upon the III were as follows:

- For the case P_r=-50dBm, the IQ diagram was similar to that of the random noise. Due to attenuation (path loss), the radar spectrum floor was bordering the receiver sensitivity, hence the resulted IQ graph was centered around zero, justifying the noise alone with $Ie^{j\theta}$=0 in 3.1.

- As the P_r was increased to -30 dBm, we saw "circular ring" formation around the center. There was a clear distinction in the sizes of IQ diagrams when compared with P_r of -50 dBm and -30 dBm.

As we increased the P_r or in other words INR (Interference to noise ratio), the circular ring's radius also increased. Therefore it could be proposed that increase in the size of ring was the result of the increase in the power or amplitude of the radar signal I. Thus, looking at the circular ring radius one could evaluate the amplitude of the radar pulse.

Note: The oscillators of VSG for the radar pulse transmission and SA were not locked, hence run at a different unsynchronized frequency, which caused phase variation.

3.3   Test for Joint Radar-Communications Sytem

In previous cases, we analyzed the radar and communications system exclusively. This section includes the combination of the two cases 3.1 and 3.2 and analyzes the impact of a radar pulse train (as interference) in a BPSK modulated communications system. The equation of the joint system of the radar at the communications receiver could be rewritten as $R = S + Ie^{j\theta} + N$.

Since both the radar and communications system's parameter would individually contribute to the received signal (4), it was important to look at the possible combinations of the variables. We performed an evaluation of various sub-cases in this section and also proposed some ways which aided reducing the impact of the interference.
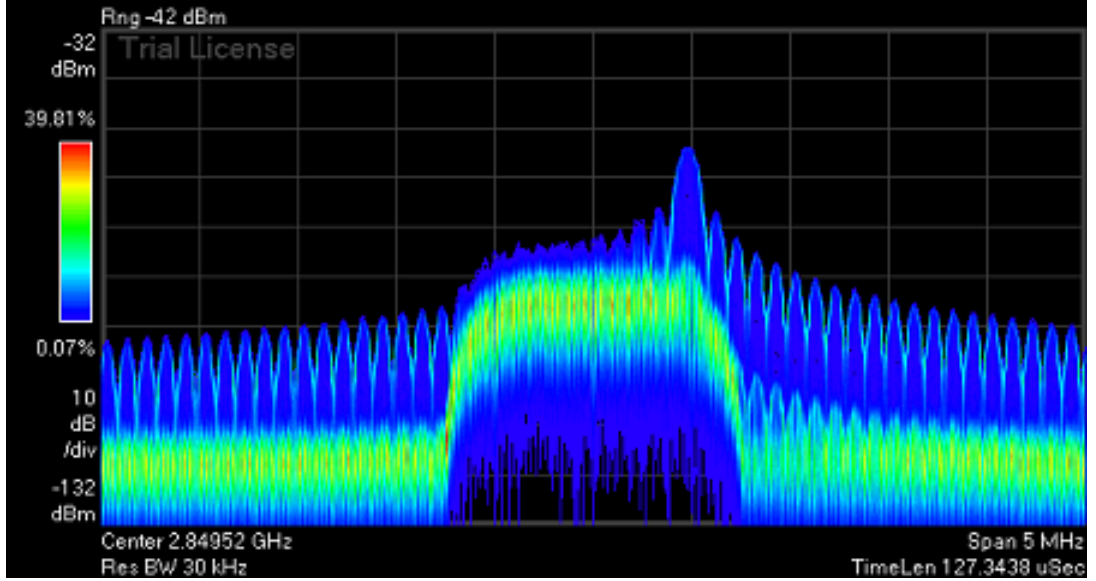
Figure 4: The real-time spectrum (leverages overlapping FFTs) of a communications system at F_c=2.84952 GHz with rectangular radar pulse centered at F_r=2.85 GHz.

3.3.0.1 IQ, BER & EVM Analysis for Different P_r(INR) and P_c(SNR) variation (τ_R, T_{PRI}=constant)

Radar signal strength is an important aspect in determining its impact in a communications receiver. In section 3.2.0.1, we noticed how a radar pulse could have different circular ring size depending upon its amplitude I. Thus, here we will look at the variable radar signal strength P_r values for a different values of P_c with τ_R=10 μs and T_{PRI}=200 μs were kept constant. Looking at the different cases as shown in IV we seek some compelling results:

- IQ diagram illustrated symmetric "circular rings" centered around the two points equidistant from the reference point I,Q=(0,0), and separated by a distance d.

- With the increase in the radar power P_r for a fixed P_c, the receiver exhibited an increase in the radius R of two "circular rings". For example, in the IV, for P_c=-35 dBm, the value of R for the "circular rings" in the IQ diagram increased as P_r was increased from -20 dBm to -10 dBm.

- There was a significant rise in the values of BER and EVM% as the value of P_r was increased for a fixed P_c. For example, the BER increased from 4.0×10^{-3} to 2.1×10^{-2} with a -10 dBm power change of radar signal in IV.
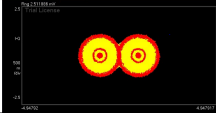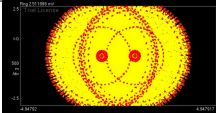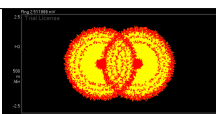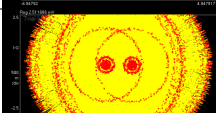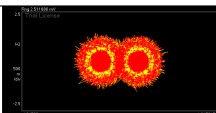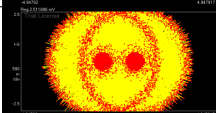
Note: The value of EVM% is not fixed for a particular BER, it might vary depending upon the setup and conditions.

The periodic trend of the increase in the BER and the size of the circular rings centered around the two IQ points could be interpreted as follows:

- The formation of the "circular rings" centered around origin was explained in section 3.2.0.1. Therefore, from 1.7 it could be explained that the circular rings were shifted to the two IQ points because of the presence of communications signal with its amplitude υ. Thus, the amplitude υ decides the location of the two "circular rings" or their separation distance d. Likewise, the value of I decided the radius R of the circular rings. Simply, we observed that the value of R and BER were proportional to the difference P_c-P_r.

Thus, looking at the IQ constellation, it could be proposed that the radar's interference impact depends on the size of the circular rings. The larger the size, the more impact it will have on the commu-

TABLE IV: Evalutation of BER and EVM%

P_r(dBm)	EVM %	BER	IQ Diagram
P_c=-35 dBm			
-20	22.7	4.0×10^{-3}	
-10	54.8	2.1×10^{-2}	
P_c=-45 dBm			
-25	35.3	1.7×10^{-2}	
-15	81.8	4.8×10^{-1}	
P_c=-55 dBm			
-40	30.6	4.9×10^{-3}	
-30	57.5	1.9×10^{-2}	

nications system. A system with an appropriate power level could be chosen to have a minimum effect in a co-existence system.

3.3.0.2 IQ & BER Analysis for T_{PRI} variation (P_c, P_r, τ_R= constant)

One of the interesting direction to look at was variation in pulse repetition interval. Exciting outcomes were observed when T_{PRI} was varied keeping the P_c, P_r and τ_R constant, considering in mind the last used setup.

- V shows "Digital Persistence" which superimposes multiple waveforms on the same view and is useful for viewing complex or time changing waveform. For example, in V, our time domain baseband signal "faded" away or in another words it was less "persistent" when T_{PRI} was increased from 200 μs to 400 μs.

- With the increase in T_{PRI}, we observed the decrease in BER. For example there is a high margin of difference in the BER when T_{PRI} is doubled in V. Interestingly, it also could be approximated from the data that BER and T_{PRI} followed an inverse linear relation as

$$BER\,(PRI = T_x) \approx \frac{1}{\ell}BER\,(PRI = \ell \times x) \tag{3.2}$$

where ℓ=constant, T_x=varied pulse repetition interval time in seconds and BER(PRI=x) denotes the value of BER when PRI is x seconds.

- The constellation diagram in V, we observed that the circular rings "scattered" and became "less dense".

  Note: The IQ diagram shows the circular rings size R and distance d between them for different cases to be of an almost equal size, which proves the point we proposed in 3.2.0.1 that R was dependent on the value of P_r.
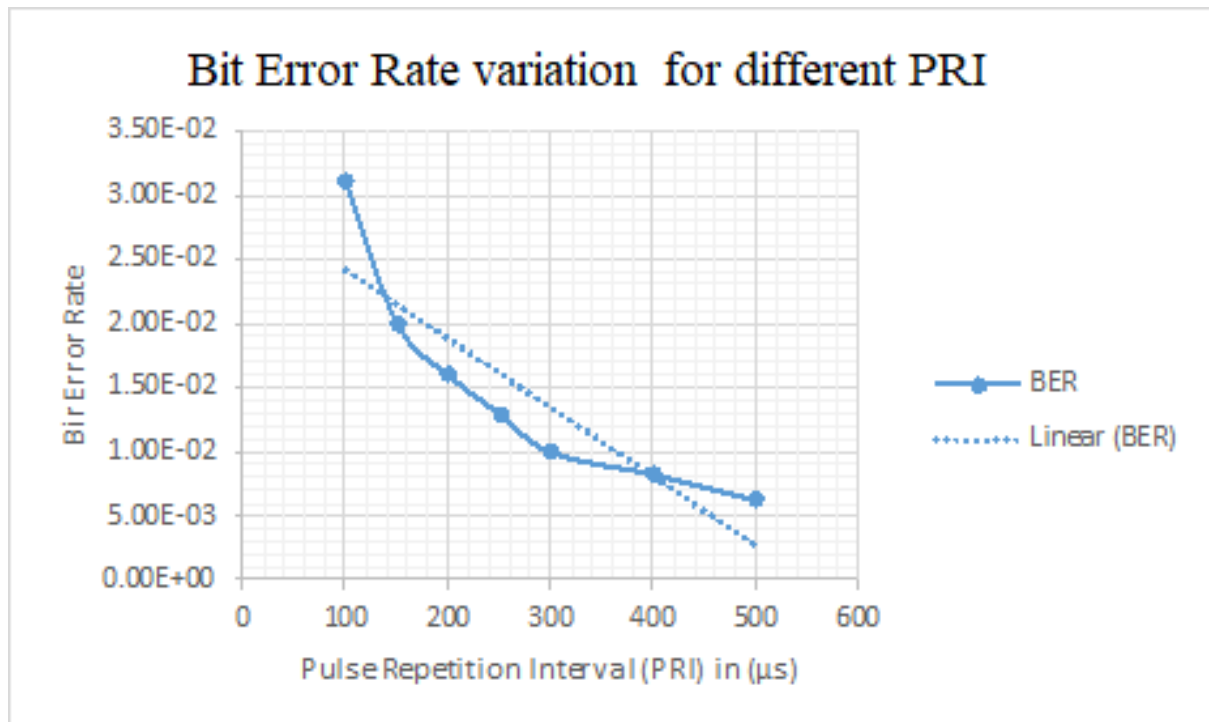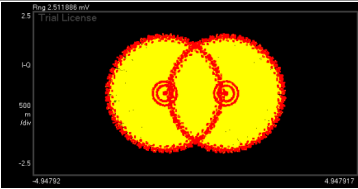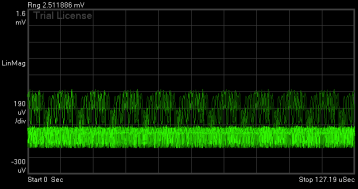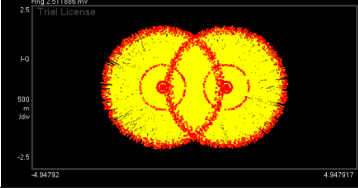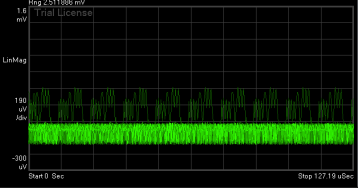
Figure 5: BER versus T_{PRI} variation showing that as T_{PRI} increases, BER decreases. An average linear BER was approximated in the figure which depicts the negative slope of the graph.

Simply put, the effect of the radar decreases if we increase the T_{PRI} as the probability of the radar hitting the communications system with amplitude υ would be less. Thus, selecting a radar T_{PRI} wisely could help in eliminating or reducing its impact as an interference.

TABLE V: BER Analysis for Varying T_{PRI} using IQ and Digital Persistence of Joint Radar-Communications System

T_{PRI}	BER	IQ Diagram	Digital Persistence
200 μs	1.6×10^{-2}		
400 μs	8.3×10^{-3}		

3.3.0.3   IQ, Spectrum & BER Analysis for F_r variations (P_c, P_r, τ_R, T_R=constant)

Practical communications system with radar interference are complex system but requires co-existence strategies with the limited bandwidth available. This section deals with selecting an appropriate center frequency F_r of the radar such that the BER could be minimized.

From 1.7, we know that at the communications receiver, the radar signals or pulse train is downconverted to the communication center frequency F_c along with the signal of interest. This downconverted signal is then passed through a bandpass/IF filter which discriminates the unwanted bandwidth of interest. In order to avoid any effect of interference, the radar signal should fall as far away as possible from the bandwidth of interest of the communication signal.

We did an experimental setup, similar to previous cases where we kept the values of $\tau_R=10 \ \mu s$, $T_{PRI}=200 \ \mu s$ and $F_c=2.849520$ GHz with $B_c=1$ MHz (with 0.5 RRC filter coefficient). But in this case, we varied the value of F_r, keeping the signal powers constant. VI clearly distinguishes the effect of varying F_r on the BER of the communications system.
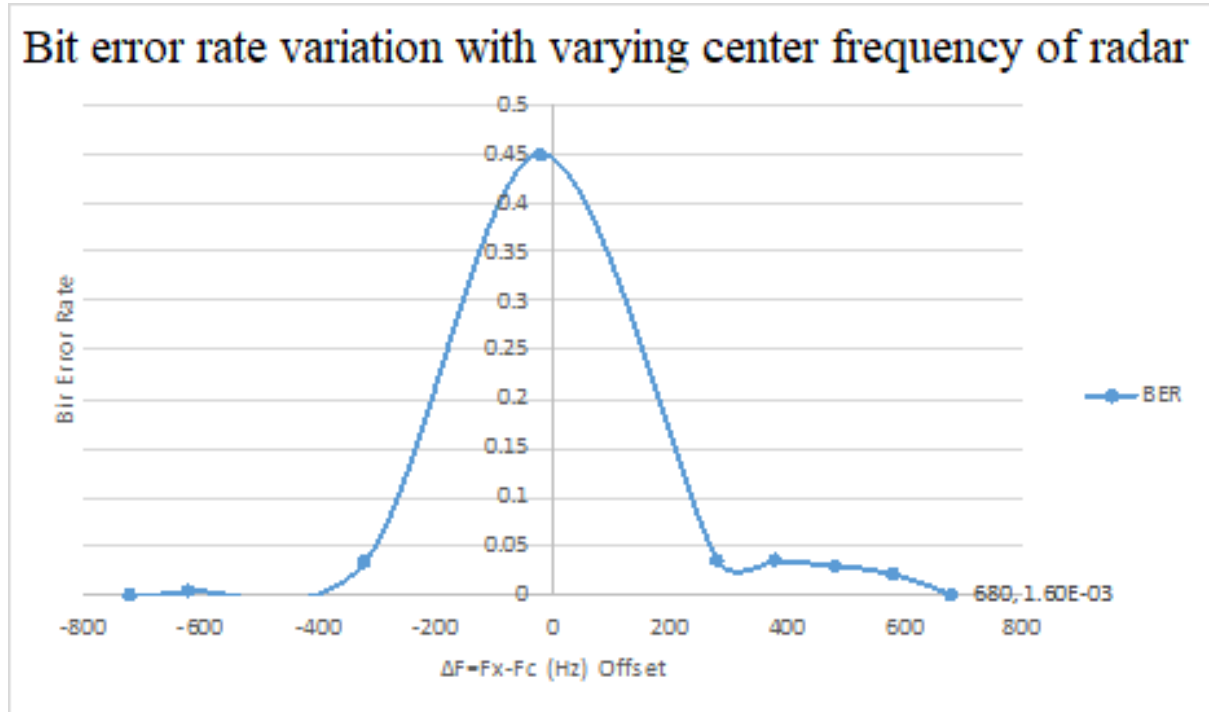

Figure 6: BER variation for different values of F_r. As the radar center frequency shifts away from F_c, BER decreases.

We observe that as we bring our radar frequency F_r closer to our central frequency F_c of communications signal, BER increased. Furthermore:

- The radius R of the circular rings increased as we move F_r closer to the F_c of communications system. As expected the distance d between the circular rings was constant for all the different cases as we did not vary the value of P_c. For example, in VI, the circular rings radius R was larger for when ΔF=-620 Hz as compared to ΔF=-280 Hz.

- The system followed the symmetry, i.e., the IQ diagram looked similar when the ΔF was varied by the same amount to the left and right w.r.t. the center frequency F_c. For example, in VI, IQ diagram was almost similar for ΔF=-620 Hz and ΔF=+580 Hz.

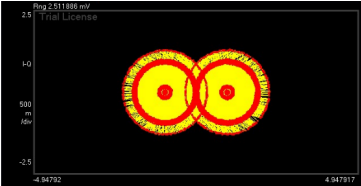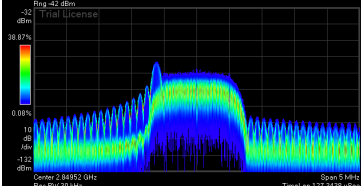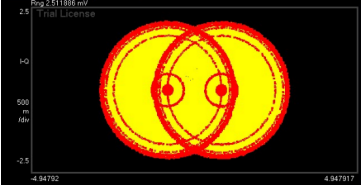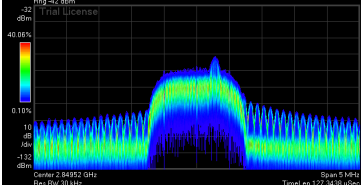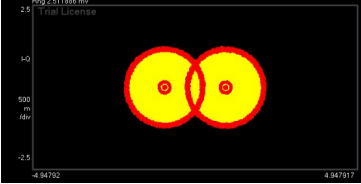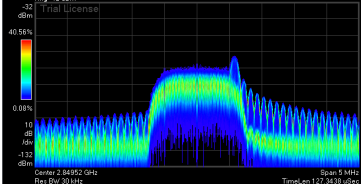The harmonics of rectangular radar pulse had lower amplitude values and hence when the radar signal was moved away from the center frequency F_c, these harmonics tend to act as an interferer, rather than the radar pulse with amplitude I, to the communications system in our required bandwidth of interest. Thus, this was the reason for the less BER when ΔF was increased.

3.3.0.4   IQ & Spectrum Analysis for Bandwidth (B_r, B_c) Variation ($\mathbf{P_c}$, $\mathbf{P_r}$, T_R=Fixed)

Lastly, we evaluated the compelling relationship between the bandwidth of radar B_r, B_c and the BER of the system displayed in VII.
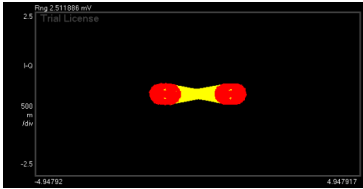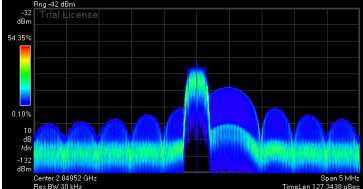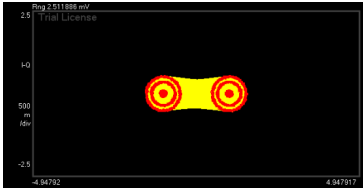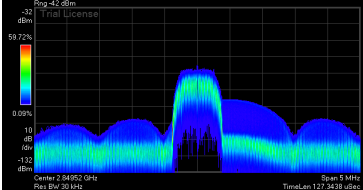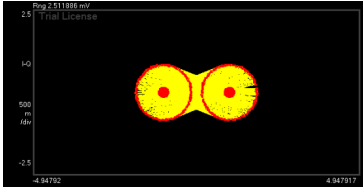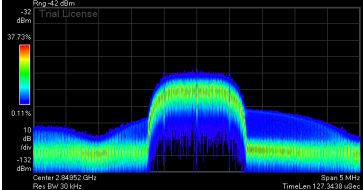
For a rectangular radar pulse $B_r = \frac{1}{\tau_R}$ Hz. For this case, we observed the consistency in the BER values if the bandwidth of both the communications signal and the radar signals were altered by the same amount. For example, in VII, we took a reference bandwidth B_c=B_r=500 KHz for the communications and the radar signal, respectively and observed the effect on BER. We varied both bandwidths simulta-

TABLE VI: BER Analysis for Varying Radar Frequency using IQ and Power Spectrum for Joint Radar-Communications Setup .

ΔF (Hz)	BER	IQ Diagram	Power Spectrum
-620	4.4×10^{-3}		
+280	3.6×10^{-2}		
+580	2.2×10^{-2}		

neously to half and twice of the reference value and observed that the BER was unaffected (which was "error free" in this case).

TABLE VII: Bandwidth Variation and BER Analysis for Joint Radar-Communications System.

B_c	B_r	IQ Diagram	Power Spectrum
$\times 0.5$	$\times 0.5$		
$\times 1$	$\times 1$		
$\times 2$	$\times 2$		

CHAPTER 4

EVALUATION FOR DIFFERENT RADAR PULSES

In this section, analytical results were compared with the simulated and the experimental results, and the evaluation were done with respect to the marginal and joint PMFs. For the case of experimental setup, only a rectangular radar pulse was considered. For the other pulse shapes, JSD values were compared between analytical and simulation model with some reference values.

4.1   Case A: Rectangular radar pulse

For evaluation purposes, we considered the rectangular radar waveform A(t) with pulse width τ_R and pulse repetition interval T_{PRI}. It is upconverted at a frequency F_r. This passband signal is then down-converted at communications system frequency F_c. Values of each variable are as shown in VIII which were taken as per the experimental model. From VIII, the rectangular time-domain radar waveform A(t) was plotted and is shown in 8. Following the same values, the PMFs was evaluated.

7 shows the real time spectrum of a rectangular radar pulse. At the right top window, "Mkr1Δ2 481 250 Hz" denotes the difference in the carrier frequencies of radar and communications system. The communications system was turned off so as to analyze our radar pulse for the PMFs. Keysight 89600 VSA software was used to extract the data from the signal analyzer to MATLAB and then compared with the other setup.
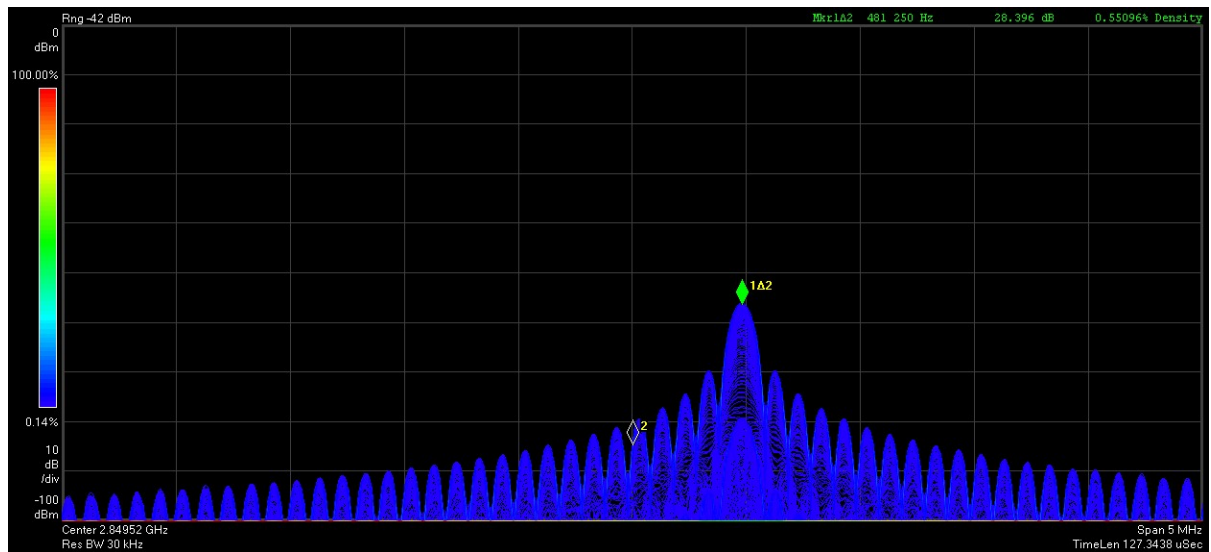
Figure 7: 2.85 GHz centered rectangular radar pulse real time spectrum (which shows cumulative history for different time instance) at communications receiver with with F_c=2.849520 GHz, Transmitted power = 0 dBm, $\tau_R = 10\ \mu$s and $T_{PRI} = 200\ \mu$s.

TABLE VIII: Rectangular radar pulse Variable values

Variables	Values
F_c	2.849520 GHz
F_r	2.85 GHz
τ_R	10 μs
T_{PRI}	200 μs
A	-30 dBm
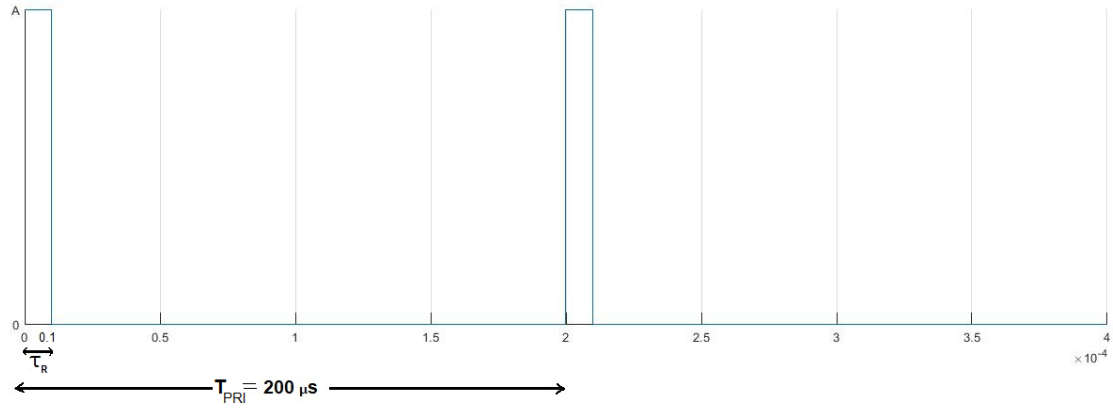
Figure 8: Rectangular pulse radar $A(t)$ with an amplitude A, $\tau_R = 10$ μs and $T_{PRI} = 200$ μs and $N=2$.

4.1.1   Marginal PMFs

From 2.15 and 2.16, PMF of the radar's amplitude and phase were plotted and were compared with the simulated as well as the experimental results. The unknown values were taken from the VIII for this experiment. Thus, 9 and 10 display the amplitude and radar PMF for the three cases, respectively.
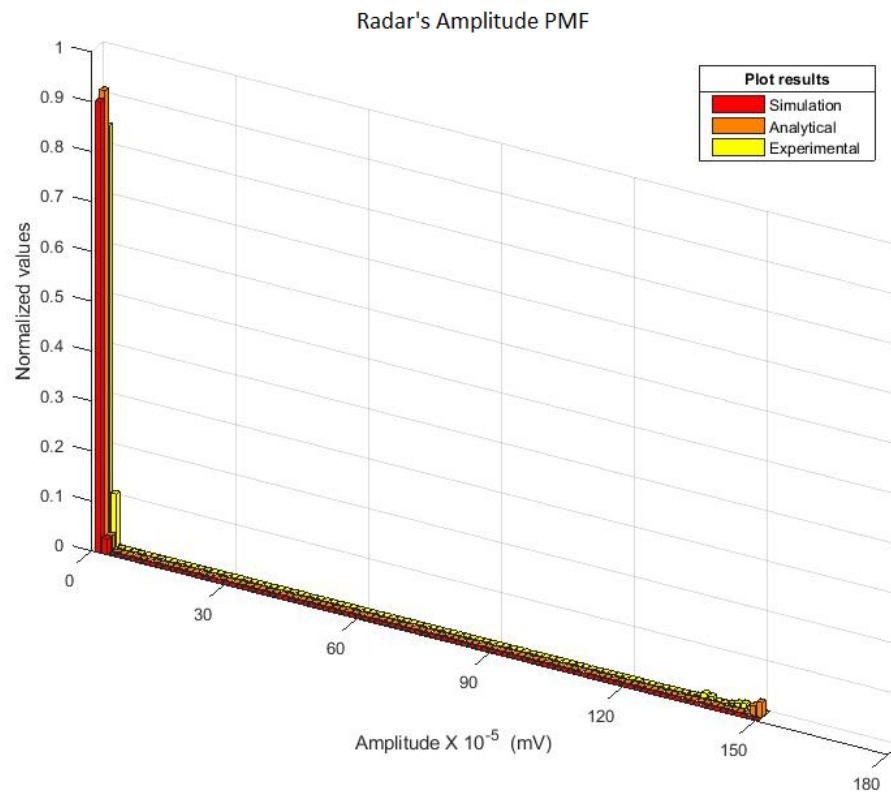
Figure 9: Comparison of radar's amplitude PMFs of experimental, analytical and simulation results.
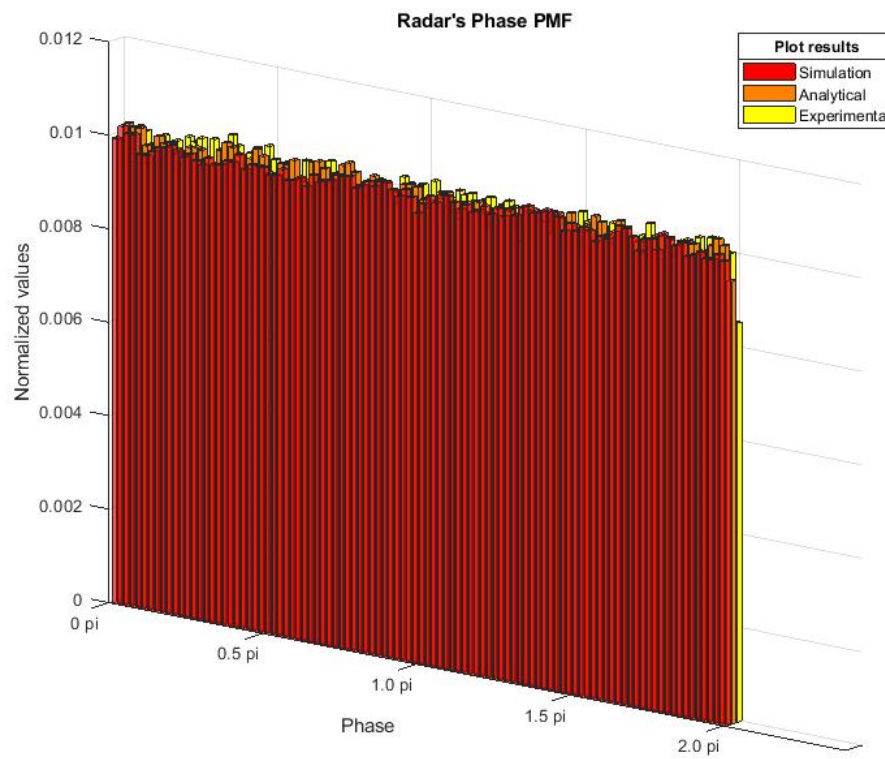
Figure 10: Comparison of radar's phase PMFs of experimental, analytical and simulation results.

Also, to individually describe the level of matching (i.e. how well it matches to the proposed setup),

JSD was calculated for marginal PMF's, i.e. for the radar amplitude and phase.

Therefore defining:

$JSDamp_{sim}$ = JSD of radar's amplitude PMFs between simulated and analytical results.

$JSDamp_{exp}$ = JSD of radar's amplitude PMFs between experimental and analytical results.

$JSDphase_{sim}$ = JSD of radar's phase PMFs between simulated and analytical results.

$JSDphase_{exp}$ = JSD of radar's phase PMFs between experimental and analytical results.

The values obtained for $JSDamp_{sim}$, $JSDamp_{exp}$, $JSDphase_{sim}$ and $JSDphase_{exp}$ were 7.04×10^{-3}, 1.02×10^{-2}, 3.06×10^{-5} and 4.08×10^{-5} respectively.

Note: Possible reasons for the $JSDamp_{exp}$ values slightly higher were due to no assumption of the rise and fall time of the rectangular pulse in the real-time (experimental) system.

4.1.2 Joint PMF

The joint PMF from 2.17 was used to generate 11. Due to the large number of mass points in the PMFs, we opted to show only theoretical results graphically. However, to quantify the accuracy of the theoretical findings we used the the Jensen–Shannon divergence (JSD) to measure the distance between the simulated and the analytical joint PMFs (JSD_{sim}), as well as between the experimental and the analytical joint PMFs (JSD_{exp}) . The JSD is a distance metric that is calculated using the Kullback–Leibler divergence (KLD)(15) between two bivariate distributions (P and Q) of the RVs A and θ.

The JSD values matched closely with each other which can be concluded from the values of JSD_{sim} = 6.34×10^{-3} and JSD_{exp} = 4.04×10^{-3}. Thus, it was claimed that the analytical model matched to
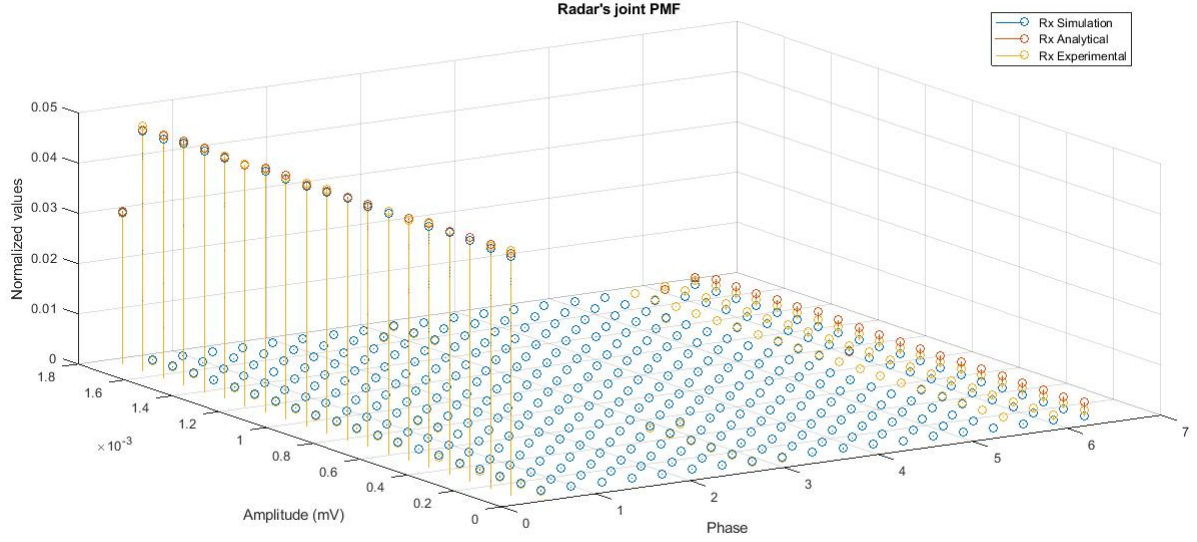
Figure 11: Comparison of joint radar's PMFs of experimental, analytical and simulation results.

a great extent with the simulation model and the experimental setup. Different cases with different radar pulse shape will be studied further, but it will not include the experimental values as discussed previously.

4.2 Case B: DME radar pair pulse

DME (16) (10) is a prominent radar system used to determine the slant distance of an aircraft to a ground station. For this purpose, DME pulse pair or gaussian shaped RF double pulses are transmitted by the aircraft to the ground station and, after a defined delay the ground station sends the pulses back again.

In our case, DME pulse pair acted as an interference to the communications system. An example of a DME radar pulse pair is shown in 12.

Figure 12: DME pulse pair radar $A(\text{t})$ with pulse spacing $\Delta t = 12\ \mu$s, pulse width of one pulse 3.5 μs $\pm$ 0.5 μs and $T_{PRI} = 50\ \mu$s.

4.2.1   Marginal PMFs

A generalized DME pulse pair are defined by 4.1.

$$A_{DME}(t) = \frac{1}{\sqrt{2\pi\sigma^2}} \left(e^{-\frac{t+\frac{\Delta t}{2}}{2\sigma^2}} + e^{-\frac{t-\frac{\Delta t}{2}}{2\sigma^2}} \right) \tag{4.1}$$

where,

$$\Delta t = \text{pulse pair spacing,}$$

$$\text{and } \sigma^2 = \text{variance of the pulse.}$$

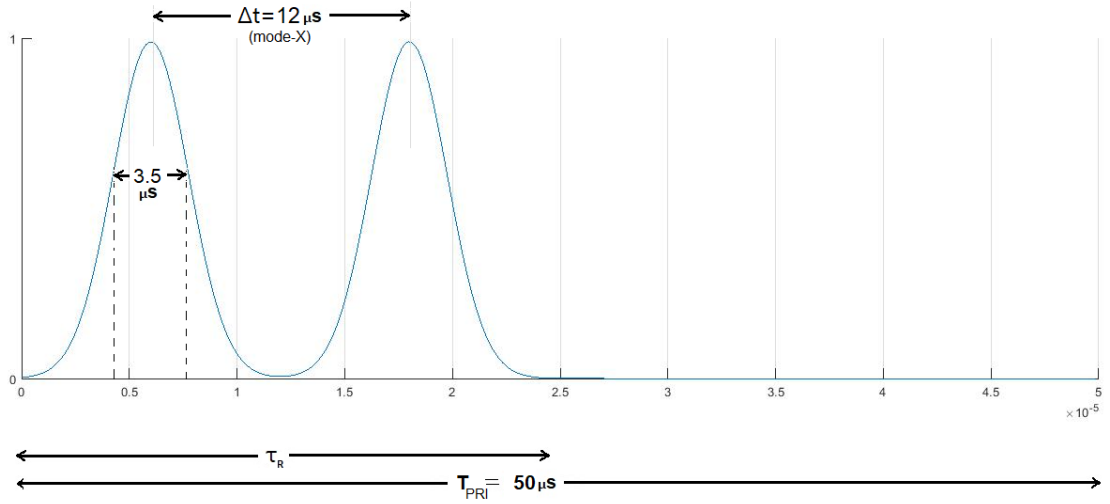To evaluate JSD for this given radar pulse shape, $\sigma = \frac{3.5}{2} \mu s \pm 0.5 \ \mu s$, mode-X pulse spacing Δt = 12 μs and T_{PRI} = 200 μs were taken. The values obtained for $JSDamp_{sim}$ and $JSDphase_{sim}$ were 2.31×10^{-4} and 4.60×10^{-5}, respectively.

4.2.2 Joint PMF

The JSD value for the joint PMF with the same values showed a good fit which can be concluded from the value of $JSD_{sim} = 3.34 \times 10^{-3}$. For the mode-Y of DME radar, which has pulse pair separation Δt = 36 μs, value of $JSD_{sim} = 3.51 \times 10^{-3}$.

4.3 Case C: Chirp radar pulse

In most of the practical radar systems (17) (18), linear FM (LFM) chirp shape is extensively used because it is more Doppler tolerant than the rectangular pulse shape. An example of a normalized LFM radar pulse as per (18) with τ_R = 100 μs and T_{PRI} = 200 μs is shown in 13.

4.3.1 Marginal PMFs

For calculating the PMFs, some of the values from VIII were taken. Using (18) as a standard pulse with a chirp radar pulse τ_R = 10 μs, T_{PRI} = 200 μs and N=15, gave $JSDamp_{sim}$ and $JSDphase_{sim}$ of 7.32×10^{-3} and 1.15×10^{-5}, respectively.
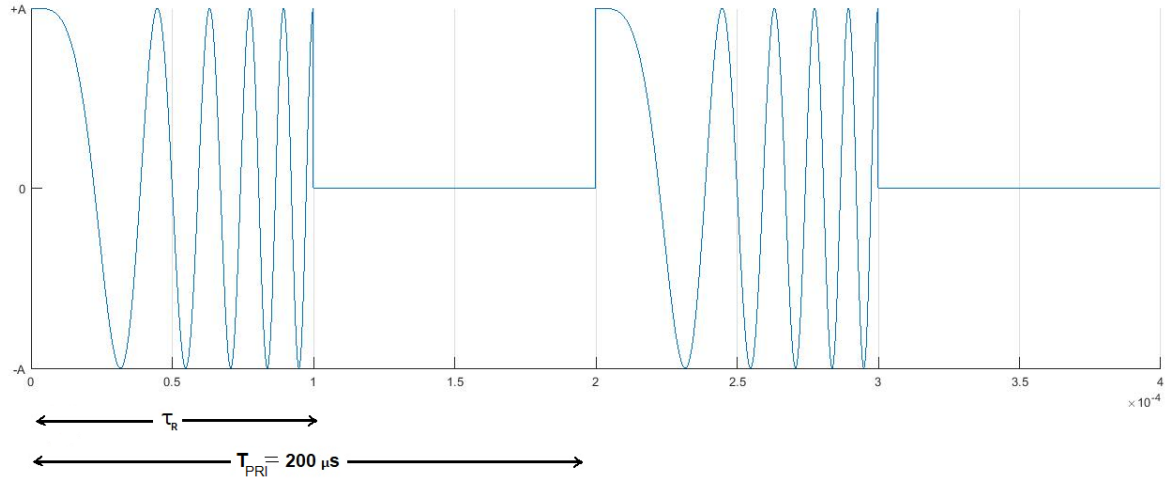
Figure 13: Real part of LFM Chirp pulse radar $A(t)$ with $\tau_R = 100$ μs and $T_{PRI} = 200$ μs and $N=2$.

4.3.2   Joint PMF

In the similar fashion as 4.1 and 4.2, the joint PMF are calculated. Therefore, using the same values of variables while calculating 4.3.1 for chirp pulse, gives $JSD_{sim} = 6.55 \times 10^{-3}$.

CHAPTER 5

CONCLUSION

An interference model was studied by using a Vector Signal Generator (VSG) as transmitter, a Signal Analyzer (SA) as a receiver with another VSG as an interference unit. Various experiments with different case studies were analyzed, which included analyses of communications system with and without radar signal, analysis of radar system alone by varying its τ_R, T_{PRI}, P_r, etc. These experimental results were validated by the theoretical analysis. The research illustrated interesting scenarios for example, we expected the BER to decrease if T_{PRI} was increased, which in research dropped from 3.1×10^{-2} to 6.3×10^{-3} when T_{PRI} was varied from 100 μs to 500 μs with τ_R, SNR, and INR constant. Also, one expects to have a higher BER if the radar frequency value is closer to the central frequency of the communications system. We observed a BER increment from 4.4×10^{-3} to 4.5×10^{-1} when ΔF offset (F_c-F_r) decreased from 620 Hz to 20 Hz. Changing the bandwidth of communications and radar system simultaneously shouldn't affect the overall BER, which was proved experimentally in our case by varying bandwidth of both the system by half and twice of the reference value.

BER was also analyzed by the IQ constellation diagram. 14 shows the formation of "circular rings" for the joint system where the circles were explained by a deterministic linearly changing phase with time. For SNR of 25 dB, we had two BER of 4.0×10^{-3} and 2.1×10^{-2} when power/amplitude of the radar pulse was varied from -20 dBm to -10 dBm, respectively. Thus, change in BER could also be interpreted by variation in the interference vector length which was related to the power/amplitude of radar pulse. The higher the value of radar power, the larger the value of radius R of circular rings.

44

Other possible cases validated by the detailed theoretical analysis for the joint setup will be considered in future.
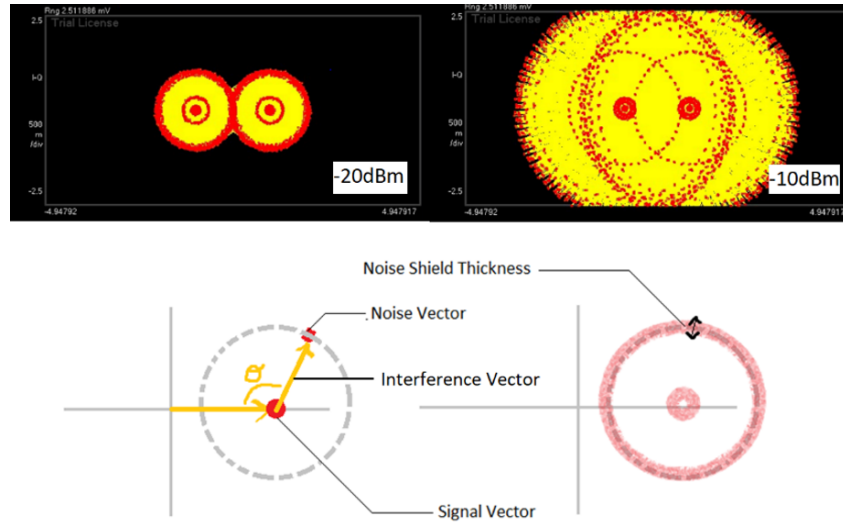
Figure 14: Shows the change in the size of the "circular rings" when interference power is increased from -20 dBm to -10 dBm(top left to top right) for a constant P_c. The bottom figure shows the cause for the circular rings and "rings width" using a vector diagram.

From the three cases 4.1, 4.2 and 4.3, values of JSD for different setup concluded the viable model which showed promising results. The mean value of $JSDamp_{sim}$, $JSDphase_{sim}$ and JSD_{sim} for the different cases were 4.86×10^{-3}, 2.93×10^{-5} and 5.46×10^{-3} , respectively. This indicates that the derived expression for the PMFs closely matched its simulated PMFs as claimed in (12). Also, this research was

able to prove the extension of (12) by involving real-time experimental. This could be concluded from the the mean values of $JSDamp_{exp}$, , $JSDphase_{exp}$ and JSD_{exp} that equals 1.02×10^{-2}, 4.08×10^{-5} and 4.04×10^{-3}, respectively for multiple iterations.

CITED LITERATURE

1. Shajaiah, H., Abdelhadi, A., and Clancy, C.: Spectrum sharing approach between radar and communication systems and its impact on radar's detectable target parameters. In 2015 IEEE 81st Vehicular Technology Conference (VTC Spring), pages 1–6, May 2015.

2. Mehrnoush, M. and Roy, S.: Interference mitigation in coexistence of wlan network with radar. In 2017 IEEE Radar Conference (RadarConf), pages 0257–0262, May 2017.

3. Clark, C. L.: LabVIEW digital signal processing. Tata McGraw-Hill Education, 2005.

4. Johnson, C. R. and Sethares, W. A.: Telecommunication breakdown: concepts of communication transmitted via software defined radio. Vol. 1. Prentice Hall, 2004.

5. Heuel, S., McCarthy, D., and Shavit, Y.: Test and measurement of coexistence between s-band radar and mobile networks. In 2016 26th International Conference Radioelektronika (RADIOELEKTRONIKA), pages 1–4, April 2016.

6. Nartasilpa, N., Tuninetti, D., Devroye, N., and Erricolo, D.: On the error rate of a communication system suffering from additive radar interference. In 2016 IEEE Global Communications Conference (GLOBECOM), pages 1–6, Dec 2016.

7. Nartasilpa, N., Tuninetti, D., Devroye, N., and Erricolo, D.: Let's share commrad: Effect of radar interference on an uncoded data communication system. In 2016 IEEE Radar Conference (RadarConf), pages 1–5, May 2016.

8. Nartasilpa, N., Shahi, S., Salim, A., Tuninetti, D., Devroye, N., Erricolo, D., Zilz, D. P., and Bell, M. R.: Let's share commrad: Co-existing communications and radar systems. In 2018 IEEE Radar Conference (RadarConf18), pages 1278–1283, April 2018.

9. Erricolo, D., Griffiths, H., Teng, L., Wicks, M. C., and Monte, L. L.: On the spectrum sharing between radar and communication systems. In 2014 International Conference on Electromagnetics in Advanced Applications (ICEAA), pages 890–893, Aug 2014.

10. Saaifan, K. A., Elshahed, A. M., and Henkel, W.: Cancelation of distance measuring equipment interference for aeronautical communications. IEEE Transactions on Aerospace and Electronic Systems, 53(6):3104–3114, 2017.

11. Tuninetti, D., Devroye, N., and Erricolo, D.: Characterization of the effect of radar interference on an uncoded data communication system. In 2016 USNC-URSI Radio Science Meeting, pages 19–20, June 2016.

12. Salim, A., Tuninetti, D., Devroye, N., and Erricolo, D.: Modeling the interference of pulsed radar signals in OFDM-based communications systems. In 2017 IEEE Radar Conference (RadarConf), pages 0657–0662, May 2017.

13. Endres, D. M. and Schindelin, J. E.: A new metric for probability distributions. IEEE Transactions on Information Theory, 49(7):1858–1860, July 2003.

14. Fuglede, B. and Topsoe, F.: Jensen-shannon divergence and hilbert space embedding. In International Symposium onInformation Theory, 2004. ISIT 2004. Proceedings., pages 31–, June 2004.

15. Kullback, S. and Leibler, R. A.: On information and sufficiency. Ann. Math. Statist., 22(1):79–86, March 1951.

16. Zhang, Q., Zheng, Y., Wilson, S. G., Fisher, J. R., and Bradley, R.: Excision of distance measuring equipment interference from radio astronomy signals. The astronomical journal, 129(6):2933, 2005.

17. Hegazy, A., Mosaad, M., and M hassan, A.: FMCW software defined radar for range and speed estimation, August 2016.

18. Roberton, M. and Brown, E.: Integrated radar and communications based on chirped spread-spectrum techniques. In Microwave Symposium Digest, 2003 IEEE MTT-S International, volume 1, pages 611–614. IEEE, 2003.

Manas Nyati

Education	M.S. Electrical and Computer Engineering University of Illinois at Chicago	2015 – 2018
	B.Tech. Electronics and Communications Engineering Rajasthan Technical University	2011 – 2015
Awards	Nokia TLC Award Pfizer Scholarship Department of Science and Technology Scholarship Department TFW Scholarship Academic Medal & Excellency Award	
Experience	Small Cell RF Hardware Engineer Intern at Nokia Research student at Andrew Electromagnetics Laboratory Teaching Assistant at ECE department for various courses	
Projects	EM Scattering Analysis using ANSYS HFSS at 2.4GHz Real-Time Communication on NI-USRP Platform Physical Layer Simulation of an LTE-OFDM System Wireless Robot with the Fractal Antenna (Microcontroller 8051)	